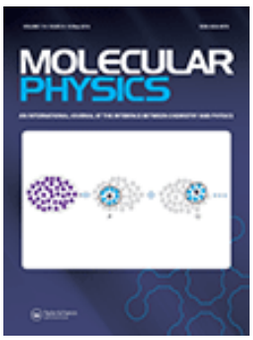

Taylor & Francis
Taylor & Francis Group

Molecular Physics

An International Journal at the Interface Between Chemistry and Physics

ISSN: 0026-8976 (Print) 1362-3028 (Online) Journal homepage: https://www.tandfonline.com/loi/tmph20

Understanding the structure and dynamical properties of stretched water by molecular dynamics simulation

Xiaowei Liu, Wei Wei, Mingbing Wu, Kang Liu & Song Li

To cite this article: Xiaowei Liu, Wei Wei, Mingbing Wu, Kang Liu & Song Li (2019): Understanding the structure and dynamical properties of stretched water by molecular dynamics simulation, Molecular Physics, DOI: 10.1080/00268976.2019.1669835

To link to this article: https://doi.org/10.1080/00268976.2019.1669835

MOLECULAR PHYSICS
https://doi.org/10.1080/00268976.2019.1669835

Taylor & Francis
Taylor & Francis Group

CUMMINGS SPECIAL ISSUE

Understanding the structure and dynamical properties of stretched water by molecular dynamics simulation

Xiaowei Liu[a]*, Wei Wei[a,b]*, Mingbing Wu[a], Kang Liu[c] and Song Li [a]

[a]State Key Laboratory of Coal Combustion, School of Energy and Power Engineering, Huazhong University of Science and Technology, Wuhan, People's Republic of China; [b]School of Chemistry and Chemical Engineering, Huazhong University of Science and Technology, Wuhan, People's Republic of China; [c]MOE Key Laboratory of Hydraulic Machinery Transients, School of Power and Mechanical Engineering, Wuhan University, Wuhan, People's Republic of China

ABSTRACT

Stretched water can sustain a large extent of stretching owing to the strong cohesion force prior to cavitation. However, the impacts of the stretching extent on the structure and dynamic properties of water is rarely investigated. In this work, molecular dynamics (MD) simulation was performed to explore the structure and dynamical properties of stretched water under varying stretching extents (i.e. evaporation coefficient). It was revealed that stretched water was more ordered under stretching and the ordering was enhanced with the increase of stretching extent. Moreover, the hydrogen bond was prolonged under stretching, accompanied with the decreased diffusion coefficients. However, the suddenly decreased structure ordering and the increased diffusion from $\varepsilon_N = 0.106$ to $\varepsilon_N = 0.121$ prior to cavitation was observed, which could be ascribed to the small cavity size of heterogeneous water phase that cannot satisfy the requirement for cavitation. This work may provide helpful insights into the molecular behaviours of water under stretching.

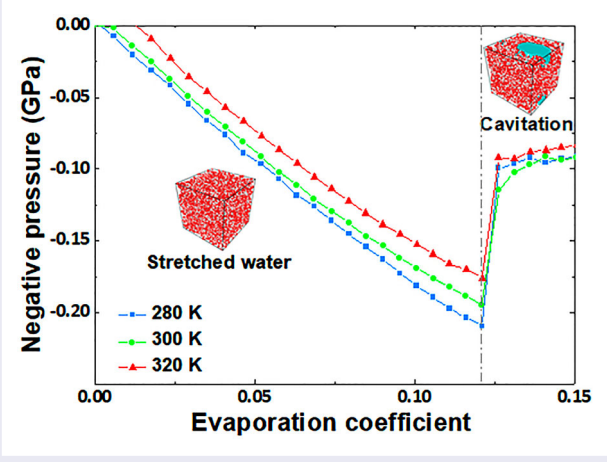

ARTICLE HISTORY
Received 30 April 2019
Accepted 11 September 2019

KEYWORDS
Stretched water; structure ordering; diffusion; heterogeneous; cavity

Introduction

Owing to the strong cohesion force of water under stretching, stretched water could withstand highly negative pressure [1]. The extremely metastable state of stretched water has been involved in many significant nature processes. For example, the transpiration of water from roots to the leaves of a tree can be attributed to the stretched water under negative pressure [2]. Experimental investigations have indicated that water in certain plants can reach pressures down to about −10 MPa [3]. In another case, large flow velocity and acceleration or fluctuations in the pressure of turbulent flows around propellers will stretch the water periodically and may cause cavitation. The subsequent collapse of cav-

CONTACT Song Li songli@hust.edu.cn State Key Laboratory of Coal Combustion, School of Energy and Power Engineering, Huazhong University of Science and Technology, Wuhan, People's Republic of China; Kang Liu kang.liu@whu.edu.cn MOE Key Laboratory of Hydraulic Machinery Transients, School of Power and Mechanical Engineering,Wuhan University, Wuhan, People's Republic of China
*These two authors contributed equally to this work.

itation bubbles during this process usually leads to severe damages to propeller blades [4–6]. Besides, negative pressure of stretched water has been recently identified as a possible reason of the collapse of porous materials during desorption [7], sonocrystallization by ultrasonic vibration [8], rain droplet freezing [8] and the pressure denaturation of protein [9]. Apart from natural phenomena, developing novel techniques to accelerate the heat and mass transfer of water powered by the negative pressure of stretched water has been firstly proposed [10].

Nevertheless, the properties of stretched water under negative pressure still remains largely unexplored. Classical nucleation theory (CNT), the most popular theory describing the pressure of stretched water is under controversy. According to CNT, the maximum negative pressure that water can sustain was approximately 160 MPa (equal to −160 MPa when considered as absolute pressure) at room temperature [11]. However, the values of negative pressure experimentally measured by various methods including acoustic method [12], metastable vapour-liquid equilibration [10], Berthelot tube [13], quartz inclusion [14], centrifugation [15] are all inevitably much lower than the CNT predicted results, which varies from −0.1 MPa to about −140 MPa. Therefore, the current experiment techniques still cannot accurately measure the negative pressure of stretched water, and the discrepancy between experimentally measured and theoretically predicted negative pressures remains elusive.

Given the limitation of current experimental techniques, molecular dynamics (MD) simulation is a suitable tool to reveal the microscopic structure and dynamical properties of stretched water. MD simulation has been frequently used to investigate the properties of water in the metastable state [16–18]. However, a few MD simulations has been reported on stretched water [19,20]. Most of these studies investigated the properties of stretched water by reducing the density of water, in which cavitation commonly occurs, leading to the different behaviours from stretched water. Therefore, in this work, we performed MD simulation to investigate the impacts of stretching extent on the structure and dynamical properties of water at varying temperatures.

Simulation details

Classical all-atom MD simulations were performed in LAMMPS [21] using TIP4P/2005 water model [22], which has been validated for describing the behaviours of stretched water [19,23,24]. The cutoff distance is 13 Å for both LJ and electrostatic interaction. The particle–particle particle-mesh (PPPM) algorithm [25] was adopted to compute long-range Coulombic interaction. The time integration scheme closely follows the time reversible measure-preserving Verlet and rRESPA integrators derived by Tuckerman et al. [26] with a time step of 1 fs. The simulation cubic box contains 5000 water molecules with periodic boundary conditions (PBCs) applied in all three dimensions. The simulation temperature is kept at 280, 300 and 320 K, respectively, via Nose–Hoover thermostat. The pressure is controlled by Nose–Hoover barostat. Each simulation is initially equilibrated under NPT ensemble at 1 bar for 4 ns. In order to simulate the stretched water, similar to the experimental process of metastable vapour-liquid equilibration, we removed a number of water molecules gradually from the initial water box to generate different stretched extents. To quantitively describe the stretching extent, we introduced the evaporation coefficient (ε_N) defined as follows.

$$\varepsilon_N = \frac{\Delta N}{N} \tag{1}$$

where N represents the initial number of water molecules in our simulation box, ΔN means the number of water molecules that was removed from the initial system. Each box of stretched water was simulated under NVT ensemble for 0.5 ns to calculate the corresponding negative pressure P using Equation (2).

$$P = \frac{Nk_BT}{V} + \frac{\sum_i^N r_i \cdot f_i}{3V} \tag{2}$$

where N is the number of atoms in the system, k_B is the Boltzmann constant, T is the temperature, and V is the system volume. The second term is the virial, where r_i and f_i are the position and force vector of atom i.

In order to quantitatively describe the structure order of water under stretching, we calculated the tetrahedral order parameter q [27] by using the four neighbouring water molecules defined by Equation (3).

$$q = 1 - \frac{3}{8}\sum_{j=1}^{3}\sum_{k=j+1}^{4}(\cos\psi_{jk} + \frac{1}{3}) \tag{3}$$

where ψ_{jk} is the angle formed by the vectors formed by the oxygen atoms j and k of neighbouring water molecules under consideration. The average q is obtained from Equation (4).

$$q = \frac{1}{N}\sum_{i=1}^{N} q_i \tag{4}$$

The average value of q varies from 0 (in an ideal gas) to 1 (in a perfect tetrahedral network).

The hydrogen bond kinetics of stretched water are characterised by hydrogen bond autocorrelation function

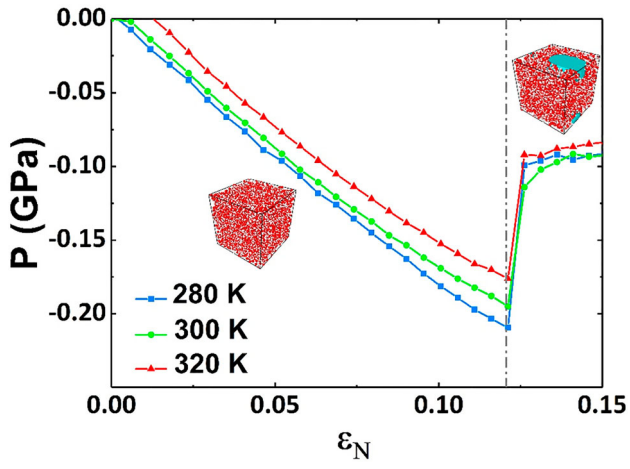

Figure 1. Negative pressure of stretched water obtained through evaporation from MD simulations at 298 K, 300 K and 320 K.

C(t) [27] defined as Equation (5).

$$C(t) = \frac{h(0)h(t)}{h} \tag{5}$$

where $h(t)$ is the hydrogen bond population operator, which has a value of 1 when the particular tagged pair atoms 1 and 2 are bonded and 0 otherwise. The average number of hydrogen bonds in an equilibrium fluid of N water molecules is 1/2 N(N-1)⟨ h⟩ , where ⟨ h⟩ denotes as the average of $h(t)$. The function is the probability of the existing hydrogen bond at time t.

Self-diffusion coefficient (D) of water molecules can be calculated using the Einstein equation of Equation (6).

$$D = \frac{1}{6}\lim_{t\to\infty}\frac{\mathrm{dMSD}(t)}{\mathrm{d}t} \tag{6}$$

$$\mathrm{MSD}(t) = \frac{1}{N}\sum_{i=1}^{n}|r_i(t) - r_i(0)|^2 \tag{7}$$

where $r_i(t)$ is the position vector of molecule i at time t. The bracket ⟨ ⟩ indicates the ensemble average. Finite size correction was not applied for self-diffusion coefficient because of the constant box size during evaporation of MD simulations, thus leading to identical errors for each system.

Results and discussion

Figure 1 shows the negative pressure of stretched water of varying evaporation coefficients (ε_N) at different temperatures. As evaporation coefficient increases, the value of negative pressure continuously increases until a maximum followed by the sudden decrease with the occurring of the cavitation and the formation of vapour bubbles (highlighted in the snapshot of Figure 1). Stretched water could withstand the high negative pressure under the lower temperature at the same evaporation coefficient. According to Figure 1, water went through two stages: stretching state during which water remains homogeneous without remarkable voids and cavitation during which water is in heterogeneous state with the formation and growth of bubbles. The cavitation stage has been studied for long time, including bubble nucleation at negative pressure [28], morphology of bubble growth [29], dynamics of cavitation bubble or molecular mechanism of cavitation [30] using both experiments and simulations. In this work, we mainly focused on the stretching state and chose the stretched states at varying evaporation coefficients ($\varepsilon_N = 0.000$, 0.063, 0.106, 0.121) from MD simulations for further analysis of structural properties and dynamical properties. It should be noted that $\varepsilon_N = 0.000$, 0.063, 0.106 represent the homogenous state of stretched water, while $\varepsilon_N = 0.121$ indicates heterogeneous water.

Table 1. The locations of the first and second peaks of RDF with different evaporation coefficients (ε_N) at 300 K.

Peaks	$\varepsilon_N = 0.000$	$\varepsilon_N = 0.063$	$\varepsilon_N = 0.106$	$\varepsilon_N = 0.121$
the first peak	2.77 Å	2.77 Å	2.79 Å	2.79 Å
the second peak	4.44 Å	4.52 Å	4.55 Å	4.55 Å

Table 2. The locations of the second peak of RDF with different evaporation coefficients (ε_N) at 280, 300 and 320 K.

Peak	Temperature	$\varepsilon_N = 0.000$	$\varepsilon_N = 0.063$	$\varepsilon_N = 0.106$
the second peak	280 K	4.44 Å	4.51 Å	4.55 Å
	300 K	4.44 Å	4.52 Å	4.55 Å
	320 K	4.44 Å	4.53 Å	4.57 Å

First of all, we analysed the oxygen-oxygen radial distribution function $g_{oo}(r)$ of stretched water under different stretched states. It was revealed that $g_{oo}(r)$ of water exhibited more pronounced oscillations under negative pressures (Figure 2a), implicating more structured water. As shown in Tables 1 and 2, with the evaporation coefficient increases, the first peak intensity is enhanced with the slight shift of the peak location ($r = 2.77$ Å to $r = 2.79$ Å). The location of the second peak slightly shifts from $r = 4.44$ Å to $r = 4.55$ Å. Compared with the effect of highly positive pressure on the structure of liquid water reported before [31,32], negative pressure of stretched water imposes the completely opposite influence. Firstly, the obvious reduction in the peak intensity of RDF has been observed under large positive pressure [33]. Secondly, it has been proved that increasing positive pressure modifies the structure of the water shell by compacting more water molecules into the water shell. On the other hand, the peak intensity decreases with the increase of temperature as shown in Figure 2(b-c).

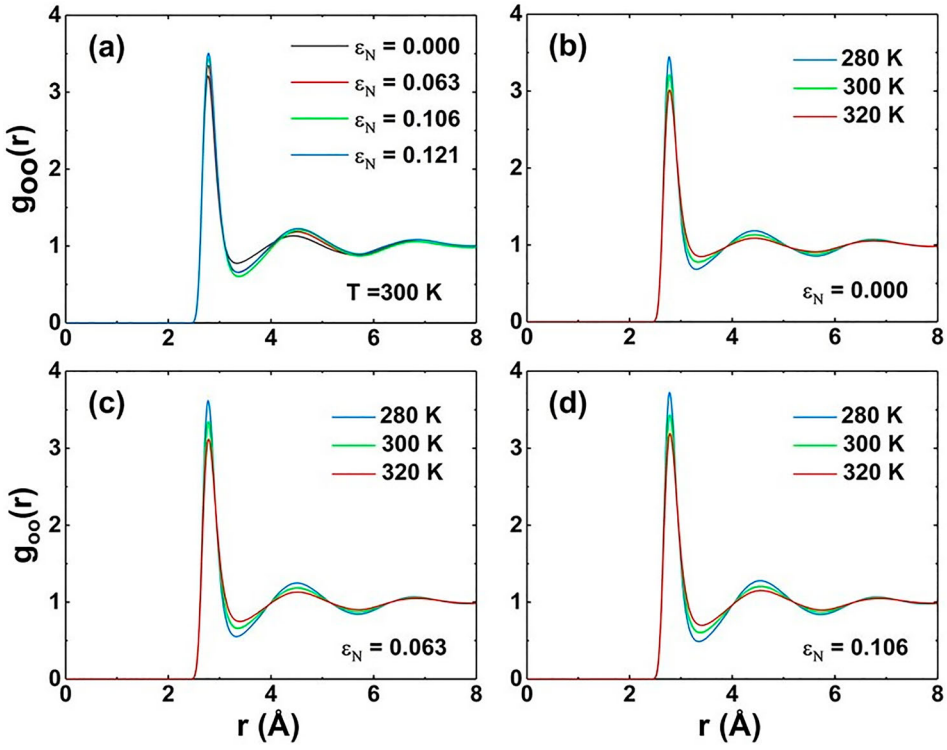

Figure 2. Radial distribution function of O-O pairs of water with different evaporation coefficients at 280, 300 and 320 K.

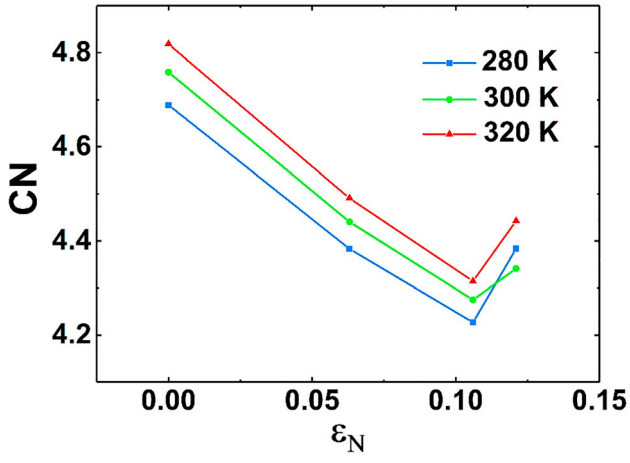

Figure 3. The coordination numbers of water molecules in the first water shell with different evaporation coefficients (ε_N) at 280, 300 and 320 K.

It suggests that stretching enhances the order of water structure, especially at low temperatures.

According to the definition of the first water shell ($r = 3.4$ Å), the coordination number (CN) of water molecules in the first water shell was calculated as shown in Figure 3. The coordination number of water molecules within the first water shell decreases as the evaporation coefficient increases, suggesting that stretching tends to pull more and more water molecules out from the first water shell. The coordination number approaches to 4 at $\varepsilon_N = 0.106$, implicating the enhanced tetrahedral arrangement of water molecules at negative pressures. This feature is consistent with the more ordered structure observed from the radial distribution function of Figure 2. With the increase of stretching extent, the bubble is supposed to be initially formed within the inter-shell region of water due to the weak interaction of inter-shell water molecules. The higher coordination number of water molecules in the shells indicates the smaller number of water molecules is likely to be found between two water shells, as well as the weaker interaction between water shells. Therefore, The formation of bubbles occurs at lower negative pressure for $T = 320$ K than that for $T = 300$ K or 280 K as shown in Figure 1. However, CN increases as the evaporation coefficient goes up from 0.106 to 0.121, which will be discussed latter Figure 4.

To further elucidate the tetrahedral arrangement of water under stretching, tetrahedral order parameter q of water under varying evaporation coefficients is calculated as shown in Figure 3. It is found that the distribution of tetrahedral order parameter probability of stretched water is a bimodal curve at 300 K (Figure 3a), which is consistent with previous reports [27,34]. With the increase of the evaporation coefficient, the low-q peak (unstructured) gradually diminishes and a high-q peak intensity is increased and accompanied with a shift of peaks towards the high q value regardless

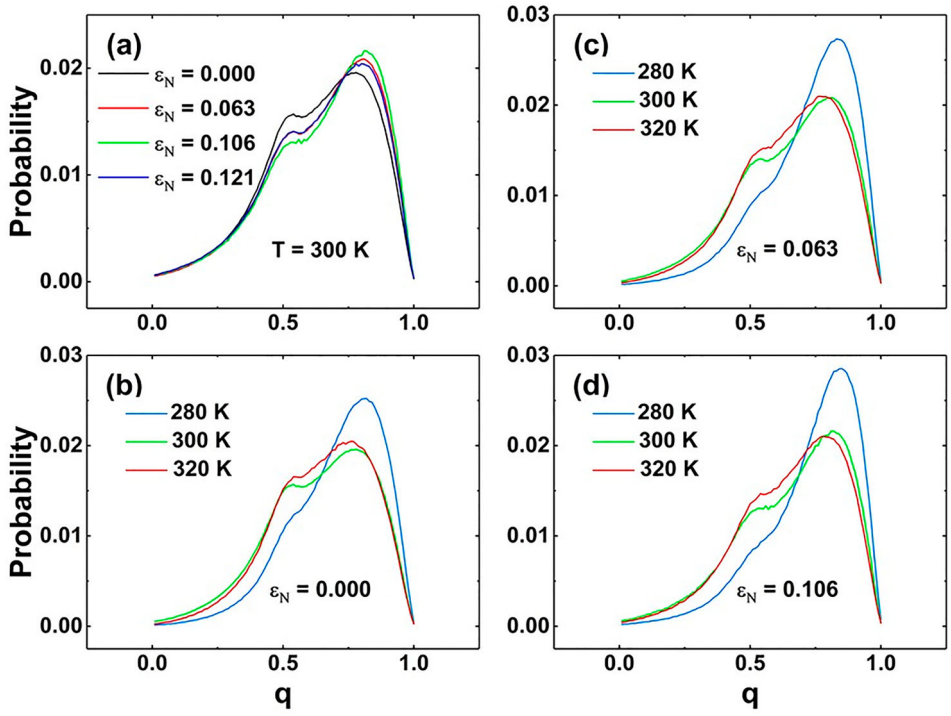

Figure 4. The tetrahedral order parameter q with different evaporation coefficients (ε_N) at 280, 300 and 320 K.

of the temperature, indicating the enhanced tetrahedral arrangement of water molecules under stretching. Nonetheless, at $\varepsilon_N = 0.121$, the distribution of q is similar to the distribution of q at $\varepsilon_N = 0.063$. This transition is in agreement with the anomaly observed in the coordination number of water molecules in the first water shell of Figure 3. With the decrease of the temperature, the tetrahedral order of water molecules was greatly enhanced (Figure 3b–d), which was more remarkable than the influence of evaporation coefficient.

In addition, we explored the hydrogen bond dynamics of stretched water. The standard definition of a hydrogen bond is applied in our work, which satisfies three criteria: O. ..O distance is less than 3.4 Å, H. ..O distance is less than 2.5 Å, and the ∠HOO is no more than 30°. Hydrogen bond dynamics can be characterised by the hydrogen bond lifetime obtained from autocorrelation function of the hydrogen bond. Intermolecular hydrogen bond lifetime is usually short, resulting from the fast vibrational and librational motions of the hydrogen bonded molecules. As shown in Figure 5(a), the autocorrelation function of hydrogen bonds under stretched conditions (i.e. negative pressure) decays slower than un-stretched water, which is more significant with the increase of ε_N, indicating the extended lifetime of hydrogen bond under stretching. Such a tendency is similar to the impacts of temperature, in which the lower the temperature, the longer the hydrogen bond lifetime. In other words, the hydrogen bond network is more stable under stretching, especially at low temperatures, which may be correlated with the enhanced tetrahedral arrangement of stretched water. The hydrogen bond lifetime constant ($C(\tau) = e^{-1}$) is provided in Table 3 for more quantitative comparison, from which the hydrogen lifetime increases with evaporation coefficients until $\varepsilon_N = 0.106$.

Table 3. The hydrogen bond lifetime constant τ with different evaporation coefficients (ε_N) at 280, 300 and 320 K.

Temperature	$\varepsilon_N = 0.000$	$\varepsilon_N = 0.063$	$\varepsilon_N = 0.106$	$\varepsilon_N = 0.121$
280 K	5.8 ps	8.8 ps	10.9 ps	9.0 ps
300 K	3.5 ps	4.2 ps	5.1 ps	5.2 ps
320 K	2.2 ps	2.6 ps	3.0 ps	2.6 ps

It is noticed that the impacts of negative pressure imposed on structural organisation of water is similar to the effects of adding hydrophobic solutes on the local structure of water [35,36]. It has reported that adding hydrophobic solutes into water reduced the local density and enhanced the structure order of water shells, eventually resulting in the decreased mobility of water[37]. Thus, the decreased mobility of water under negative pressures is expected as shown in Figure 6. With the increase of ε_N, self-diffusion coefficient is reduced until $\varepsilon_N = 0.106$, after which the diffusion was slightly increased. This feature is more remarkable at low temperature (i.e. 280 K). However, with the increasing temperature, the influence of stretching on the diffusion of water molecules is less significant. In fact, the reduced diffusion of stretched water at lower density has been previously

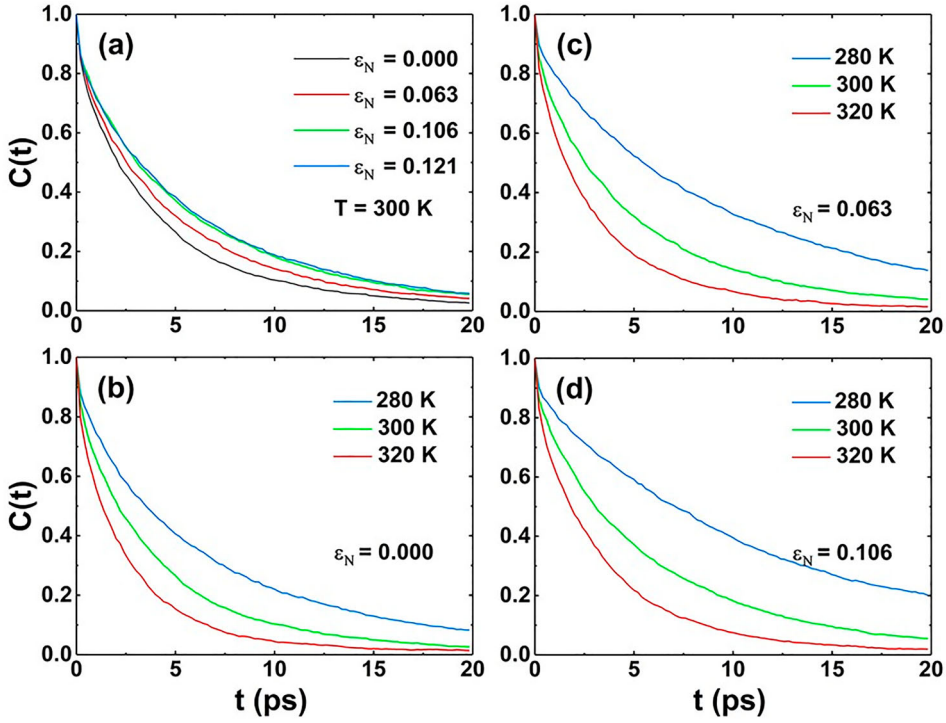

Figure 5. Hydrogen bond correlation function with different evaporation coefficients (ε_N) at 280, 300 and 320 K.

reported using molecular simulation [20,24], in which the self-diffusion coefficient firstly decreased as density decreased and reached a minimum value near the ice density. Further decrease in density caused the increased diffusion, which is more pronounced at low temperature. However, the similar dependence of self-diffusion coefficient on the evaporation coefficient or negative pressures is observed. The trend in diffusion coefficient can be attributed to the more structured water and stable hydrogen bond network under stretching, which is favourable for the rigidity of structure organisation and the lower the vibrational and librational motions of the hydrogen bonded molecules.

The sudden increase in the diffusion coefficient at the maximum stretching coefficient is an anomaly, similar to the tendency observed in coordination number, tetrahedral arrangement and hydrogen bond lifetime. In order to understand the anomaly in both structural and dynamical properties of water at $\varepsilon_N = 0.121$ (critical point of negative pressure), we calculated the void fraction of water under varying pressures as shown in Figure 7. It is revealed that the void fraction remarkably increases when ε_N increased from 0.106–0.121, suggesting the transition from homogenous to heterogeneous phases as demonstrated by the morphology of cavities (Figure 7a-b) under varying stretching states (i.e. negative pressure). Further excessive stretching or decreasing pressure will result in the emergence of massive cavities and the existing vapour voids (Figure 7c)

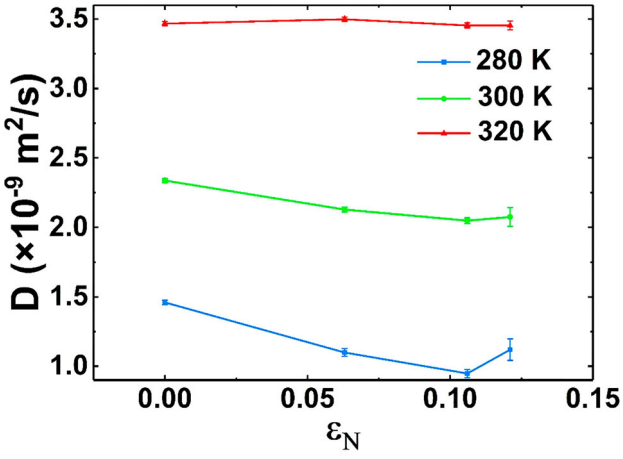

Figure 6. Self-diffusion coefficient with different evaporation coefficients (ε_N) at 280, 300 and 320 K obtained from three independent simulations.

disrupt the local structure of metastable water. Thus, the tetrahedral arrangement also shows a decreasing tendency, similar to the shortened hydrogen bond lifetime, leading to increased diffusion. Nevertheless, no cavitation occurs at $\varepsilon_N = 0.121$ according to Figure 1 regardless of the heterogenous phase of water. According to the classical nucleation theory (CNT) [4,38], a cavity can only survive and grow to a stable bubble (Figure 7d) when it exceeds critical radial size (R_C). Before reaching that point, stretched water could withstand the higher strain as shown in Figure 1. The radius

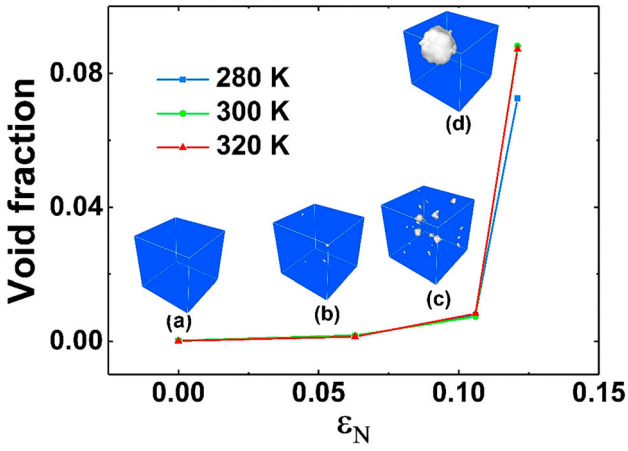

Figure 7. Simulation snapshots and void fraction with different evaporation coefficients ε_N at 280, 300 and 320 K.

of critical cavity (R_C) is calculated by the following equation:

$$R_C = \frac{2\gamma}{P_0 - P} \tag{8}$$

where γ is surface tension coefficient of water, P_0 is the saturated vapour pressure and P is the hydrostatic pressure of water. When $R > R_C$, cavities can grow larger. When $R < R_C$, cavities are unstable and may disappear. Take $T = 300$ K, $\gamma = 72$ mN/m and $P = -0.19$ GPa as an example (the value of P_0 compared with the P is small enough to be ignored), the critical cavity radius is predicted to be 0.76 nm. We also measured the cavity size at $\varepsilon_N = 0.121$ from MD simulation by 'Construct surface mesh' method using OVITO [39]. The probe sphere radius is 3.4 Å, which is the diameter of the first water shell, and the smoothing level is 8 in OVITO. The radius of cavity under −0.19 GPa at 300 K is predicted to be 0.74 nm, which is smaller than the predicted R_C of CNT theory. Therefore, no cavitation was observed at $\varepsilon_N = 0.121$ although the negative pressure $\varepsilon_N = 0.121$ has achieved the maximum.

Conclusions

In this work, we performed MD simulation of stretched water at varying temperatures. Local structure analysis was employed to investigate the influence of evaporation coefficient on. According to RDF and coordination number, it was found that more and more water molecules were pull out from the first under stretching. From tetrahedral order parameter, it is proposed that the tetrahedral arrangement is enhanced with the increasing evaporation coefficient. Hydrogen bond analysis dynamics suggests the HB network turns into a more stable state. This improved network stability thus results in a decrease in the diffusion coefficient. The anomalous properties of water under negative pressure observed in our work is attributed to the increasing cavity size prior to cavitation during the phase transition of water from homogeneous to heterogeneous. These findings may provide useful insights into water under negative pressure from the molecular level, which could further inspire experimental and theoretical studies on stretched water of the community.

Disclosure statement

No potential conflict of interest was reported by the authors.

Funding

This work was supported by the National Natural Science Foundation of China [NSFC, No. 51606081 and 51606082] and double first-class research funding of China–EU Institute for Clean and Renewable Energy (No. ICARE-RP-2018-HYDRO-001). This work was carried out at National Supercomputer Center in Shenzhen.

ORCID

Song Li http://orcid.org/0000-0003-3552-3250

References

[1] F. Caupin and A.D. Stroock, *The Stability Limit and Other Open Questions on Water at Negative Pressure* (John Wiley & Sons, Hoboken, HJ, 2013).
[2] A.D. Stroock, V.V. Pagay, M.A. Zwieniecki and N.M. Holbrook, Annu. Rev. Fluid. Mech. **46** (1), 615–642 (2014).
[3] P.F. Scholander, E.D. Bradstreet, E. Hemmingsen and H. Hammel, Science. **148** (3668), 339–346 (1965).
[4] R.E.A. Arndt, Annu. Rev. Fluid. Mech. **13** (1), 273–326 (1981).
[5] J.P. Franc and J.M. Michel, Fluid Mechanics & Its Applications. **76** (11), 1–46 (2004).
[6] Z. Pan, A. Kiyama, Y. Tagawa, D.J. Daily, S.L. Thomson, R. Hurd, and T.T. Truscott, Proc. Natl. Acad. Sci. U. S. A. **114** (32), 1702502114 (2017).
[7] B. Coasne, A. Galarneau, R.J. Pellenq and R.F. Di, Chem. Soc. Rev. **42** (9), 4141–4171 (2013).
[8] C. Marcolli, Sci. Rep. **7** (1), 16634 (2017).
[9] V. Bianco and G. Franzese, Phys. Rev. Lett. **115** (10), 1–36 (2015).
[10] T.D. Wheeler and A.D. Stroock, Nature. **455** (7210), 208 (2008).
[11] F. Caupin and E. Herbert, Comptes Rendus - Physique. **7** (9), 1000–1017 (2006).
[12] K. Davitt, A. Arvengas and F. Caupin, Epl. **90** (1), 620–625 (2010).
[13] E. Roedder, Science. **155** (3768), 1413–1417 (1967).
[14] Q. Zheng, D.J. Durben, G.H. Wolf and C.A. Angell, Science. **254** (5033), 829–832 (1991).
[15] L.J. Briggs, J. Appl. Phys. **21** (21), 721–722 (1950).
[16] J. Qvist, H. Schober and B. Halle, J. Chem. Phys. **134** (14), 1415 (2011).

[17] P. Gallo, F. Sciortino, P. Tartaglia and S.H. Chen, Phys. Rev. Lett. **76** (15), 2730–2733 (1996).
[18] P. Kumar and H.E. Stanley, J. Phys. Chem. B. **115** (48), 14269–14273 (2011).
[19] Y.E. Altabet, R.S. Singh, F.H. Stillinger and P.G. Debenedetti, Langmuir. **33** (42), 11771 (2017).
[20] P.A. Netz, F.W. Starr, H.E. Stanley and M.C. Barbosa, J. Chem. Phys. **115** (1), 344–348 (2001).
[21] S.J. Plimpton, J. Chem. Phys. **117** (1), 1–19 (1995).
[22] J.L.F. Abascal and C. Vega, J. Chem. Phys. **123** (23), 219 (2005).
[23] P. Wang, W. Gao, J. Wilkerson, K.M. Liechti, and R. Huang, Extreme. Mech. Lett. **11**, 59–67 (2016).
[24] P. M. De Hijes, E. Sanz, L. Joly, C. Valeriani, and F. Caupin, J. Chem. Phys. **149**, 094503 (2018).
[25] R.W. Hockney and J.W. Eastwood, *Computer Simulation Using Particles* (CRC Press, Boca Raton, FL, 1988).
[26] M. Tuckerman, B.J. Berne and G.J. Martyna, J. Chem. Phys. **97** (3), 1990–2001 (1992).
[27] J.R. Errington and P.G. Debenedetti, Nature. **409** (6818), 318–321 (2001).
[28] J.L. Abascal, M.A. Gonzalez, J.L. Aragones and C. Valeriani, J. Chem. Phys. **138** (8), 1561 (2013).
[29] A.V. Neimark and A. Vishnyakov, J. Chem. Phys. **122** (5), 52 (2005).
[30] G. Menzl, M.A. Gonzalez, P. Geiger, F. Caupin, J.L. Abascal, C. Valeriani and C. Dellago, Proc. Natl. Acad. Sci. U. S. A. **113** (48), 13582–13587 (2016).
[31] A.V. Okhulkov, Y.N. Demianets, Y.E. Gorbaty, A.V. Okhulkov, Y.N. Demianets and Y.E. Gorbaty, J. Chem. Phys. **100** (2), 1578–1588 (1994).
[32] A.K. Soper and M.A. Ricci, Phys.rev.Lett. **84** (13), 2881 (2000).
[33] A.K. Soper, Chem. Phys. **258** (2), 121–137 (2000).
[34] Y.I. Jhon, K.T. No and S.J. Mu, Fluid Phase Equilib. **244** (2), 160–166 (2006).
[35] A. Geiger, A. Rahman and F.H. Stillinger, J. Chem. Phys. **70** (1), 263–276 (1979).
[36] R. Dogonadze and Erika Kalman, editors, *The Chemical Physics of Solvation.Part A*. (Elsevier, Amsterdam, 1985).
[37] F. Sciortino, A. Geiger and H.E. Stanley, Nature. **354** (6350), 218–221 (1991).
[38] F. Caupin, Physical Review E Statistical Nonlinear & Soft Matter Physics. **71** (1), 051605 (2005).
[39] A. Stukowski, Modelling Simul. Mater. Sci. Eng. **18**, 015012 (2010).